Coupled third-order simplified spherical harmonics and diffusion equation–based fluorescence tomographic imaging of liver cancer

Xueli Chen
Fangfang Sun
Defu Yang
Jimin Liang

Coupled third-order simplified spherical harmonics and diffusion equation–based fluorescence tomographic imaging of liver cancer

Xueli Chen,* Fangfang Sun, Defu Yang, and Jimin Liang
Xidian University, School of Life Science and Technology, 266 Xinglong Section of Xifeng Road, Xi'an 710126, China

Abstract. For fluorescence tomographic imaging of small animals, the liver is usually regarded as a low-scattering tissue and is surrounded by adipose, kidneys, and heart, all of which have a high scattering property. This leads to a breakdown of the diffusion equation (DE)–based reconstruction method as well as a heavy computational burden for the simplified spherical harmonics equation (SP_N). Coupling the SP_N and DE provides a perfect balance between the imaging accuracy and computational burden. The coupled third-order SP_N and DE (CSDE)-based reconstruction method is developed for fluorescence tomographic imaging. This is achieved by doubly using the CSDE for the excitation and emission processes of the fluorescence propagation. At the same time, the finite-element method and hybrid multilevel regularization strategy are incorporated in inverse reconstruction. The CSDE-based reconstruction method is first demonstrated with a digital mouse-based liver cancer simulation, which reveals superior performance compared with the SP_N and DE-based methods. It is more accurate than the DE-based method and has lesser computational burden than the SP_N-based method. The feasibility of the proposed approach in applications of *in vivo* studies is also illustrated with a liver cancer mouse-based *in situ* experiment, revealing its potential application in whole-body imaging of small animals. © 2015 Society of Photo-Optical Instrumentation Engineers (SPIE) [DOI: 10.1117/1.JBO.20.9.090502]

Liver cancer is one of the most common malignancies in the world, leading to more than 600,000 deaths every year.[1] Often detected at a relatively late stage, it is increasingly difficult to cure with the existing therapies. New detection techniques are, therefore, urgently needed for the early detection and diagnosis of this aggressive disease. Fluorescence tomographic imaging (FMT) is a promising imaging modality that has been extensively applied for the early detection of malignant tumors and monitoring therapeutic response.[2,3] Because FMT can provide three-dimensional (3-D) imaging and assess for the concentration of fluorescent probes inside a living body,[4] it has great potential for the detection of *in situ* liver cancer. Researchers have devoted their efforts to the application of the FMT technique for the pharmacokinetic analysis and early detection of liver cancer.[5,6] In these studies, the diffusion equation (DE) was employed to describe the fluorescence propagation and to develop the corresponding reconstruction algorithms. For whole-body animal imaging with visible or near-infrared light, the liver is specified as low-scattering tissue that is surrounded by adipose, kidneys, heart, etc., which have a high-scattering property.[7] As a result, the DE-based FMT reconstruction algorithms are hindered by the validity assumption of DE, that is, that a highly diffuse media is required for guaranteeing its accuracy. The higher-order approximations of the radiative transfer equation have been used for describing fluorescence propagation, but they suffer from heavy computational burden.[8,9] In the authors' previous study,[10] the coupled third-order simplified spherical harmonics and diffusion equation (CSDE) was developed to describe the light propagation in tissues, which aims to balance the characteristic accuracy with the overall computational burden. In the present study, the CSDE model was extended and applied to the FMT reconstruction and relevant applications for the detection of liver cancer.

Based on the concise form of CSDE deduced in the authors' previous study,[10] the forward model for FMT reconstruction can be constructed by doubly using it in both the excitation and emission processes. In the excitation end, the excitation light source term is replaced by a Dirac delta function $\delta(r - r_s)$ with an amplitude of E; in the emission process, the light source term is the fluorescence yield $\eta\mu_{af}(r)$ that is excited by the light flux distribution Φ_x of the incident excitation light:

$$
\begin{aligned}
&-\nabla \cdot C_{k,\nabla\Phi_{1x}}(r)\nabla\Phi_{1x}(r) - \nabla \cdot C_{k,\nabla\Phi_{2x}}(r)\nabla\Phi_{2x}(r) \\
&+ C_{k,\Phi_{1x}}(r)\Phi_{1x}(r) + C_{k,\Phi_{2x}}(r)\Phi_{2x}(r) = C_{k,Sx}(r)E\delta(r - r_s) \\
&-\nabla \cdot C_{k,\nabla\Phi_{1m}}(r)\nabla\Phi_{1m}(r) - \nabla \cdot C_{k,\nabla\Phi_{2m}}(r)\nabla\Phi_{2m}(r) \\
&+ C_{k,\Phi_{1m}}(r)\Phi_{1m}(r) + C_{k,\Phi_{2m}}(r)\Phi_{2m}(r) = C_{k,Sm}(r)\Phi_x\eta\mu_{af}(r),
\end{aligned}
\tag{1}
$$

where subscripts x and m denote the excitation and emission light, respectively; $\eta\mu_{af}(r)$ is the target to be reconstructed and simplified as $X(r)$ in the following part; $C_{k,\nabla\Phi_1}(r)$, $C_{k,\nabla\Phi_2}(r)$, $C_{k,\Phi_1}(r)$, $C_{k,\Phi_2}(r)$, and $C_{k,S}(r)$ ($k = 1,2$) are constant coefficients;[10] Φ_x is defined as[8]

$$
\Phi_x = \Phi_{1x} - \frac{2}{3}\Phi_{2x},
\tag{2}
$$

where $\Phi_{kx}(k = 1, 2)$ can be calculated from the excitation part of the CSDE-based forward model.

Using the finite-element method, a linear relationship between the exiting partial current J_m at the outer boundary and the unknown fluorescent yield is established:

$$J_m = A\Phi_x X \quad = \bar{A}X, \tag{3}$$

where $\bar{A} = A\Phi_x$ is the system matrix for FMT reconstruction.

The FMT reconstruction can be achieved by calculating the fluorescent yield distribution X from boundary measurements J_m using Eq. (3). This is a typically ill-posed problem due to the insufficiency of measurements at boundary. The adaptive mesh discretization and regularization strategy have been utilized to ensure its accuracy and stability. Based on the h adaptive FEM (h-FEM), a hybrid and multilevel regularization strategy is adopted to solve the fluorescent yield distribution X from the following optimization function:

$$\hat{X} = \underset{X_k \geq 0}{\arg\min} \|\bar{A}_k X_k - J_m^{\text{meas}}\|_2^2 + \tau_k \lambda_{pk} |X_k|_p$$
$$+ (1 - \tau_k)\lambda_{2k}|X_k|_2^2, \tag{4}$$

where $\hat{X}$ is the reconstructed fluorescent yield, J_m^{meas} is the measured exiting partial current from the outer boundary, λ_{pk} and λ_{2k} are the regularization parameters for l_p-norm ($p = (0,1]$) and l_2-norm regularization terms, respectively, where subscript k represents the k'th level meth, and τ_k is the binary function, which is equal to unity when $k = 1$ and specified as zero for other cases.

For the first-level mesh, the solving domain is discretized into a uniformly coarse mesh. Compared with the whole solving domain, the fluorescent target to be reconstructed has a sparse distribution. The incomplete variables truncated conjugate gradient method for sparse reconstruction is used to solve the solution.[11] This result is regarded as a permissible region for subsequent reconstruction. Using the h-FEM, the permissible region is further discretized to a fine mesh, and a new system equation can be obtained. With respect to the permissible region, the fluorescent target distribution lacks obvious sparsity. Thus, the Landweber regularization is then conducted:[12]

$$X^{\text{iter}+1} = (I - \lambda_{2k}\bar{A}^T\bar{A})X^{\text{iter}} + \lambda_{2k}\bar{A}^T J^{\text{meas}}. \tag{5}$$

The performance of the CSDE based FMT reconstruction is first evaluated with a digital mouse-based simulation. The selected organs and relevant optical properties are listed in Table 1, where the optical properties for excitation light are calculated at the wavelength of 680 nm, and those for emission light are calculated at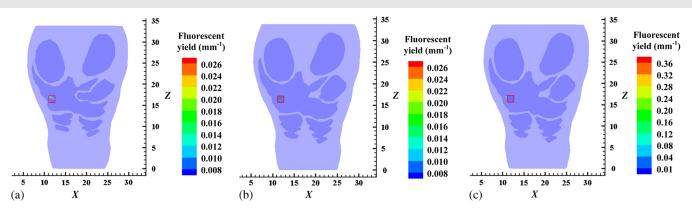 the wavelength of 710 nm.[7] A cylinder with a 0.8-mm radius and 1.6-mm height was placed in the liver with its center at (11.9, 6.4, 16.4) mm to simulate the fluorescent target. In the simulation, the fluorescent yield of the fluorescent target was specified as 0.05 mm^{-1}. Under the excitation at 18 positions in sequence, synthetic surface measurements were calculated on the fine mesh of 132,202 tetrahedrons and 24,906 nodes using the SP$_3$ model. For each excitation position, the surface light flux was measured on the opposite side with a field of view of 120 deg. Finally, a total of 18 data sets were assembled for the reconstruction of fluorescent yield.

For the inverse reconstruction, the digital mouse model was initially discretized into 15,141 tetrahedrons and 3050 nodes as the coarse-level mesh, and the ultimate mesh refined with the h-FEM has 26,399 tetrahedrons and 5035 nodes. The distribution and concentration of the fluorescent target were reconstructed using the CSDE-based reconstruction method. As the references, the SP$_3$ and DE were also used to substitute the CSDE model in the reconstruction.[8,9,12] Figure 1 illustrates the related reconstructed results of the CSDE, SP$_3$, and DE-based reconstruction methods, respectively. The actual position of the fluorescent target is outlined with a red circle and the values of the reconstructed fluorescent yield are shown with the colored bar. We find that almost the same images were recovered with both the CSDE- and SP$_3$-based reconstruction methods, which are better than that of the DE-based method. In the reconstructed image using the DE-based approach, the reconstructed elements deviated from the actual position in the way of a scattered distribution. To quantitatively analyze these results, two evaluation factors, including the localization error (LE) and the quantification error (QE), are defined to evaluate the localization and quantification results. The LE is defined as the Euclidean distance between the centers of the reconstructed and actual targets, and the QE denotes the relative error between the reconstructed and actual fluorescent yields. Although the LE obtained with the CSDE-based reconstruction method (0.85 mm) is somewhat worse than the SP$_3$-based method (0.73 mm), the difference is only 0.12 mm and is minor compared with the diameter of the target. Moreover, the same fluorescent yield is reconstructed using the CSDE- and SP$_3$-based methods (0.0279), with the same QE of 44.2%. Nevertheless, both the localization and quantification results of the CSDE-based reconstruction method are much better than those of the DE-based method. The LE of the DE-based method is 2.07 mm, which has exceeded the size of actual fluorescent target. At the same time, the reconstructed fluorescent yield is

Table 1 Optical properties of selected organs of a mouse. The optical parameters are in units of mm^{-1}.

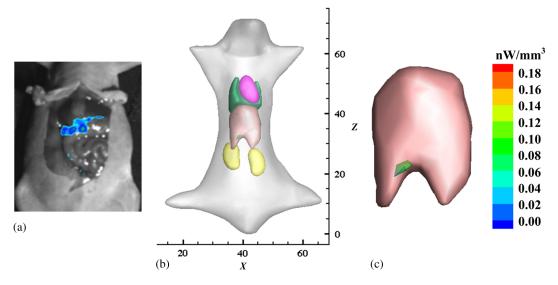| Tissue | 680 nm | | 710 nm | | 480 nm | | 525 nm | | g |
	μ_{ax}	μ'_{sx}	μ_{am}	μ'_{sm}	μ_{ax}	μ'_{sx}	μ_{am}	μ'_{sm}	
Adipose	0.0034	1.1983	0.0025	1.1712	0.032498	1.428634	0.061712	1.372970	0.94
Heart	0.0509	0.9437	0.0337	0.8872	0.481156	1.516581	0.939478	1.362374	0.85
Stomach	0.0099	1.4164	0.0070	1.3583	—	—	—	—	0.92
Liver	0.3041	0.6676	0.2005	0.6380	2.886884	0.945823	5.636813	0.874210	0.90
Kidneys	0.0571	2.2032	0.0380	2.0641	0.538899	3.635985	1.052221	3.246741	0.86
Lungs	0.1696	2.1569	0.1106	2.1081	1.376959	2.571542	2.846116	2.471347	0.94

Fig. 1 Reconstructed results using the (a) coupled third-order simplified spherical harmonics and diffusion equation, (b) SP$_3$, and (c) diffusion equation based reconstruction methods. In each panel, the actual position of the fluorescent target is outlined with a red square and the values of the reconstructed fluorescent yield are shown with the color bar.

overestimated (0.367). In the authors' previous study,[10] it was observed that the CSDE model can save time (with the value varying with the ratio of high-scattering region to the whole domain) compared with the SP$_3$ method, which reflects in the construction of system matrix $\bar{A}$. In this simulation, the time costs of the HSDE-, SP$_{3-}$, and DE-based methods for the construction of system matrix $\bar{A}$ are 666.67, 805.19, and 73.86 s, respectively. All of the results are recorded on a personal computer with 2.2 GHz Inter(R) Core(TM) i7-4702 CPU and 8.00 GB RAM. As a result, the CSDE-based method not only provides comparable accuracy in both localization and quantification as the SP$_3$-based approach, but also largely reduces its computation time, which would facilitate its wide applications in whole-body small animal imaging.

The applicability of the CSDE-based reconstruction method is then illustrated with a liver cancer based *in vivo* experiment. In the experiment, athymic male BALB/c nude mice, approximately four to five weeks old, were selected as the Xenograft models for the *in situ* liver cancer animal model. All of the animal procedures were performed in accordance with the guidance of the Institutional Animal Care and Use Committee at Peking University (Permit Number: 2011-0039). After the mice were anesthetized with sodium pentobarbital, a laparotomy was carefully performed on the mice to completely expose the liver. A cell suspension of 50 μl HCC-LM3-fLuc-GFP with the concentration of 1×10^3 cells/μl was injected into the lower left liver lobe. After brief local compression, the dissected skin and abdominal wall were closed with Prolene suture.[6]

After anesthetized by inhalation of 2% isoflorane, the mouse was mounted on the animal bed that was located on the rotation stage. By rotating the rotation stage with an equally spaced 90 deg, four views fluorescent images were acquired from mouse surface with a dual-modality FMT-CT system.[6] A 488-nm continuous wave semiconductor laser was utilized as the excitation source to illuminate the mouse surface, and a band pass filter with the central wavelength of 525 nm was used to collect the fluorescent signals. Subsequently, anatomical images were also acquired using the Micro-CT system, which provided the anatomical structure for the FMT reconstruction. After the images were acquired, the mouse was intraperitoneally

Fig. 2 Reconstructed results of the *in vivo* liver-cancer-based experiment: (a) laparotomy results with the liver exposed and imaged using bioluminescence imaging, (b) three-dimensional rendering of the reconstructed result, and (c) local enlarged image that zooms in the local area of the liver. In the figures, the colored elements describe the reconstructed distribution of the liver cancer.

injected with D-luciferin and then dissected to expose the liver for bioluminescence imaging (BLI). An intense signal can be seen from the lower left hepatic lobe, as shown in Fig. 2(a).

Prior to reconstruction, the acquired fluorescent images were mapped onto the body surface of the anatomical structure of the mouse with the self-developed light flux mapping method.[13] The segmented organs and the related optical properties for the excitation and emission light, which forms the physical model of digital mouse, are listed in Table 1. On the basis of the light flux map retrieved on the body surface and the physical model, the location and distribution of inoculated HCC-LM3-fLuc-GFP cells were reconstructed by using the CSDE-based reconstruction method. Figure 2 illustrates the localization results of the HCC-LM3-fLuc-GFP cells. Figure 2(b) shows the 3-D view of the reconstructed result, and Fig. 2(c) gives the local enlarged image at higher magnification of the area of interest within the liver. In the figures, the colored elements denote the reconstructed distribution of the liver cancer. As seen in Fig. 2, we find that the reconstructed elements resolve the location of the inoculated HCC-LM3-fLuc-GFP cells well, while maintaining good consistency with the dissected result of the BLI. The results of this experiment illustrate that the CSDE-based reconstruction method has great clinical applicability and potential for the detection of *in situ* liver cancer.

In summary, the CSDE-based reconstruction method is presented for FMT of liver cancer. The liver cancer simulation demonstrates a level of accuracy comparable to the SP_3-based reconstruction method but an improved accuracy compared with the DE-based method. Moreover, the CSDE-based reconstruction method takes less time than the SP_3-based method for constructing the system matrix.[10] The applicability of the CSDE-based reconstruction is also demonstrated with an *in vivo* liver-cancer-based experiment, which shows its great potential for the detection of *in situ* liver cancer. A generalized Delta-Eddington phase function deduced by Cong et al.[14] can also accurately model the light propagation in tissues over a wide range of optical properties and be less time consuming than the SP_N. Thus, we may try to couple the generalized Delta-Eddington phase function with the DE in the next step. Our future work will focus on its applications in a longitudinal and quantitative manner for monitoring the development of *in situ* liver cancer as well as response to drug therapy.

Acknowledgments

References

1. A. Jemal et al., "Global cancer statistics," *CA Cancer J. Clin.* **61**(2), 69–90 (2011).
2. P. Fortin et al., "Detection of brain tumors using fluorescence diffuse optical tomography and nanoparticles as contrast agents," *J. Biomed. Opt.* **17**(12), 126004 (2012).
3. S. Davisa et al., "Dynamic dual-tracer MRI-guided fluorescence tomography to quantify receptor density *in vivo*," *Proc. Nat. Acad. Sci. USA* **110**(22), 9025–9030 (2013).
4. C. Darne, Y. Lu, and E. Sevick-Muraca, "Small animal fluorescence and bioluminescence tomography: a review of approaches algorithm and technology update," *Phys. Med. Biol.* **59**(1), R1–R64 (2014).
5. G. Zhang et al., "Imaging of pharmacokinetic rates of indocyanine green in mouse liver with a hybrid fluorescence molecular tomography/x-ray computed tomography system," *J. Biomed. Opt.* **18**(4), 040505 (2013).
6. Q. Zhang et al., "Comprehensive evaluation of the anti-angiogenic and anti-neoplastic effects of endostar on liver cancer through optical molecular imaging," *PLoS One* **9**(1), e85559 (2014).
7. D. Yang et al., "Performance investigation of SP_3 and diffusion approximation for three-dimensional whole-body optical imaging of small animals," *Med. Biol. Eng. Comput.* (2015).
8. A. Klose and T. Pöschinger, "Excitation-resolved fluorescence tomography with simplified spherical harmonics equations," *Phys. Med. Biol.* **56**(5), 1443–1469 (2011).
9. L. Zhang et al., "Analytical Green's function for the fluorescence simplified spherical harmonics equations in turbid medium," *J. Biomed. Opt.* **19**(7), 070503 (2014).
10. X. Chen et al., "Hybrid simplified spherical harmonics with diffusion equation for light propagation in tissues," *Phys. Med. Biol.* **60**(16), 6305–6322 (2015).
11. X. He et al., "Sparse reconstruction for quantitative bioluminescence tomography based on the incomplete variable truncated conjugate gradient method," *Opt. Express* **18**(24), 24825–24841 (2010).
12. H. Yi et al., "Multilevel, hybrid regularization method for reconstruction of fluorescent molecular tomography," *Appl. Opt.* **51**(7), 975–986 (2012).
13. X. Chen et al., "3D reconstruction of light flux distribution on arbitrary surfaces from 2D multi-photographic images," *Opt. Express* **18**(19), 19876–19893 (2010).
14. X. Cong et al., "Integral equations of the photon fluence rate and flux based on a generalized Delta-Eddinton phase function," *J. Biomed. Opt.* **13**(2), 024016 (2008).